Latin American Journal of Solids and Structures
www.lajss.org

An accurate novel coupled field Timoshenko piezoelectric beam finite element with induced potential effects

Abstract

An accurate coupled field piezoelectric beam finite element formulation is presented. The formulation is based on First-order Shear Deformation Theory (FSDT) with layerwise electric potential. An appropriate through-thickness electric potential distribution is derived using electrostatic equilibrium equations, unlike conventional FSDT based formulations which use assumed independent layerwise linear potential distribution. The derived quadratic potential consists of a coupled term which takes care of induced potential and the associated change in stiffness, without bringing in any additional electrical degrees of freedom. It is shown that the effects of induced potential are significant when piezoelectric material dominates the structure configuration. The accurate results as predicted by a refined 2D simulation are achieved with only single layer modeling of piezolayer by present formulation. It is shown that the conventional formulations require sublayers in modeling, to reproduce the results of similar accuracy. Sublayers add additional degrees of freedom in the conventional formulations and hence increase computational cost. The accuracy of the present formulation has been verified by comparing results obtained from numerical simulation of test problems with those obtained by conventional formulations with sublayers and ANSYS 2D simulations.

Keywords

Piezoelectric, Beam, Finite elements, Coupled field, Variational formulation, Induced potential

Litesh N Sulbhewar[a, *]
P. Raveendranath[b]

[a]Research Scholar - Department of Aerospace Engineering, Indian Institute of Space Science and Techology, Thiruvananthapuram, India.

[b]Adjunct Professor - Department of Aerospace Engineering, Indian Institute of Space Science and Techology, Thiruvananthapuram, India.

[*]Author Email: liteshsulbhewar@gmail.com

1 INTRODUCTION

Piezoelectric smart structures have a unique capability to control their behaviour, by virtue of electromechanical coupling present in them (Crawley and de Luis, 1987). Piezoelectric material present in the smart structure can be used either as sensor to get the quantitative information about the subjected environment or as an actuator to implement corrective action (Chee et al., 1999). Due to

the high reliability of piezoelectric smart structures, they have become the integral part of static shape and vibration control technology. Piezoelectric smart beams are widely used in modern control technology (Benjeddou et al., 1997; 2000). Accurate numerical modeling of piezoelectric beams plays an important role in the design of these control systems (Chee et al., 1999).

Many mathematical models are available in the literature, to analyze piezoelectric beams. The very early analytical model given by Crawley and de Luis (1987) was based on uniform strain and Euler-Bernoulli beam theory, to study the effectiveness of piezoelectric material in controlling static and dynamic behaviour of beams. Closed form solutions for axial strain, curvature and natural frequencies based on Euler-Bernoulli beam theory have been provided by Abramovich and Pletner (1997). Plate and beam elements based on classical laminate theory, given by Hwang and Park (1993) and Bendary et al. (2010) can be used for static and dynamic analyses of thin smart beams. However, all these models based on classical theory neglect transverse shear and hence are inadequate for shorter and thick beams (Benjeddou et al., 1999). Zhang and Sun (1996) proposed a classical Sandwich Beam Theory (SBT) based analytical solution in which the thick core is modeled as Timoshenko beam and the relatively thin faces as Euler-Bernoulli beam. Based on SBT, Raja et al. (2002) proposed beam finite element to study the behaviour of piezoelectric smart beams. However, these SBT based models are insignificant for thick and short piezoelectric smart beams with thick piezoelectric face layers as SBT neglects shear effect in faces. Tzou and Tseng (1991) proposed a non-conforming hexahedron piezoelectric finite element by adding internal degrees of freedom to the original eight node hexahedron solid element (Tzou and Tseng, 1988), to give improved performance in thin structural analysis. Tzou and Ye (1996) developed a new laminated quadratic C^0 piezoelastic triangular shell finite element using layerwise constant shear angle theory. Robbins and Reddy (1991) proposed two Equivalent Single Layer (ESL, Euler-Bernoulli and Timoshenko) and two Layerwise (one with constant while other with layerwise linear transverse deflection through the thickness) models for integrated smart beams, which considered strain induced by piezoelectric material as applied strain. These models are without electrical degrees of freedom. Saravanos and Heyliger (1995) used the same layerwise models with electrical degrees of freedom. Donthireddy and Chandrashekhara (1996) used layerwise theory with constant through-thickness transverse deflection for parametric study of laminated beams with piezoelectric actuators. First-order Shear Deformation Theory (FSDT) based analytical closed form solutions given by Abramovich (1998), Sun and Huang (2000) and finite elements proposed by Shen (1995), Narayanan and Balamurugan (2003), Neto et al. (2009), Rathi and Khan (2012) can be used for static and dynamic analyses of surface mounted extension mode smart beams. ESL-FSDT and Higher-order Shear Deformation Theory (HSDT) based analytical solutions have been proposed by Aldraihem and Khdeir (2000) and Khdeir and Aldraihem (2001) for actuation of these extension mode beams. Also, HSDT based finite elements have been used by Peng et al. (1998), Chee et al. (1999) and Elshafei and Alraiess (2013) for static and dynamic analyses of these beams.

All the formulations mentioned above, used assumed layerwise linear through-thickness distribution of electric potential which is actually nonlinear due to induced potential effects (Benjeddou et al., 1997; Plagianakos and Saravanos, 2005; Rachmadani et al., 2005; Kapuria and Hagedorn, 2007). The induced potential increases stiffness of the piezoelectric structure. To take care of this nonlinear part, either sublayers are to be added in mathematical modeling of the piezoelectric

layer (Rachmadani et al., 2005; Chee et al., 1999) and/or higher order approximation has to be applied for through-thickness potential (Plagianakos and Saravanos, 2005; Kapuria and Hagedorn, 2007). But, the addition of sublayers and/or use of higher order polynomial approximation introduce additional electric potential degrees of freedom in the model, thus making it computationally expensive. Benjeddou et al. (1997, 2000), in their SBT based beam finite element, have derived coupled field quadratic expression for through-thickness distribution of electric potential based on Euler-Bernoulli beam theory. The higher order term in the derived expression depends on bending rotation. However, this field is inadequate where the shear effect is dominant.

In this work, an ESL-FSDT based piezoelectric extension mode beam finite element with layerwise coupled higher order through-thickness distribution of electric potential is presented. The appropriate through-thickness electric potential consistent with FSDT is derived from the electrostatic equilibrium equations. The higher order nonlinear term present in the derived expression depends on bending rotation (θ) of the beam and does not add any extra electrical degrees of freedom in the formulation. The results obtained are compared with conventional ESL-FSDT formulations with layerwise assumed linear potential (with and without sublayers in modeling) and ANSYS 2D finite element simulations. The numerical results show the importance of considering induced potential effects in the modeling. The efficiency and accuracy of the present formulation over the conventional formulations have been proved by the comparison of numerical results of test problems.

2 THEORETICAL FORMULATION

The formulation is based on ESL-FSDT for a mechanical field with layerwise electric potential. Consider the general multilayered extension mode piezoelectric smart beam as shown in Figure 1. The layer can be of conventional/composite/piezoelectric material with isotropic/specially orthotropic properties. The layers are assumed to be perfectly bonded to each other. Mechanical and electrical quantities are assumed to be small enough to apply linear theories of elasticity and piezoelectricity. Assumptions of beam theory apply.

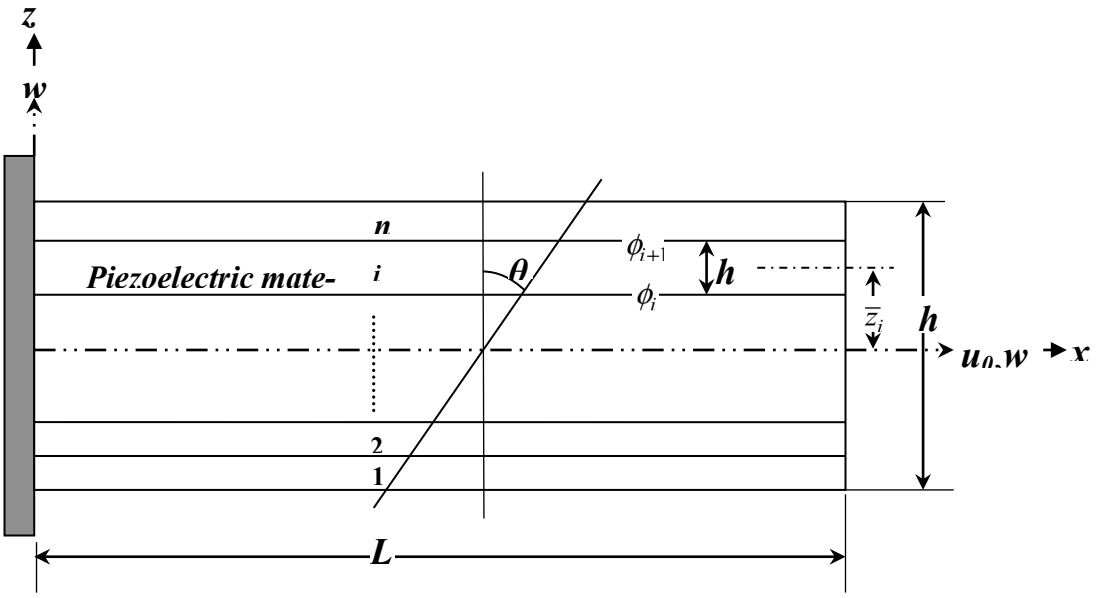

Figure 1 Geometry of a general multilayered extension mode piezoelectric smart beam.

2.1 Mechanical displacements and strains

The displacement fields in longitudinal and transverse directions for FSDT are given as:

$$u(x,z) = u_0(x) + z\theta(x) \tag{1}$$

$$w(x,z) = w_0(x) \tag{2}$$

where the mid-plane sub-functions u_0 and w_0 denote axial and transverse displacements, respectively. θ is the section rotation of the beam. Dimensions b and h denote the width and total thickness of the structure.

Axial and shear strains are found by usual strain-displacement relations as:

$$\varepsilon_x(x,z) = \frac{\partial u(x,z)}{\partial x} = u_0^{'}(x) + z\theta^{'}(x) \tag{3}$$

$$\gamma_{xz}(x,z) = \frac{\partial u(x,z)}{\partial z} + \frac{\partial w(x,z)}{\partial x} = \theta(x) + w_0^{'}(x) \tag{4}$$

where $()^{'}$ denotes $\frac{d}{dx}$.

2.2 Electric potential and electric field

The layerwise potential distribution is assumed as shown in Figure 1. The two-dimensional electric potential of i^{th} piezoelectric layer $\varphi_i(x,z)$ takes the value of ϕ_{i+1} and ϕ_i at the top and bottom faces, respectively. The electric field in transverse direction can be derived as (Benjeddou et al., 1997):

$$E_z^i = -\frac{\partial \varphi_i(x,z)}{\partial z} \tag{5}$$

3 REDUCED CONSTITUTIVE RELATIONS

The piezoelectric material with isotropic/specially orthotropic properties with axes of material symmetry parallel to beam axes is considered here. For extension mode beams, transversely poled piezoelectric material layer is subjected to transverse electric field. The elastic, piezoelectric and dielectric constants are denoted by $\mathbf{C}_{ij}, \mathbf{e}_{kj}(i,j=1.....6)$ and $\in_k (k=1,2,3)$, respectively. Coupled constitutive equations for such a material are given as:

$$\begin{bmatrix} \sigma_x \\ \sigma_y \\ \sigma_z \\ \tau_{yz} \\ \tau_{xz} \\ \tau_{xy} \\ D_x \\ D_y \\ D_z \end{bmatrix} = \begin{bmatrix} C_{11} & C_{12} & C_{13} & 0 & 0 & 0 & 0 & 0 & -e_{31} \\ C_{12} & C_{22} & C_{23} & 0 & 0 & 0 & 0 & 0 & -e_{32} \\ C_{13} & C_{23} & C_{33} & 0 & 0 & 0 & 0 & 0 & -e_{33} \\ 0 & 0 & 0 & C_{44} & 0 & 0 & 0 & -e_{24} & 0 \\ 0 & 0 & 0 & 0 & C_{55} & 0 & -e_{15} & 0 & 0 \\ 0 & 0 & 0 & 0 & 0 & C_{66} & 0 & 0 & 0 \\ 0 & 0 & 0 & 0 & e_{15} & 0 & \in_1 & 0 & 0 \\ 0 & 0 & 0 & e_{24} & 0 & 0 & 0 & \in_2 & 0 \\ e_{31} & e_{32} & e_{33} & 0 & 0 & 0 & 0 & 0 & \in_3 \end{bmatrix} \begin{bmatrix} \varepsilon_x \\ \varepsilon_y \\ \varepsilon_z \\ \gamma_{yz} \\ \gamma_{xz} \\ \gamma_{xy} \\ E_x \\ E_y \\ E_z \end{bmatrix} \tag{6}$$

where $\sigma, \tau, \varepsilon, \gamma, D$ and E denote normal stress (N/m^2), shear stress (N/m^2), normal strain, shear strain, electric displacement (C/m^2) and electric field (V/m), respectively.

For a one-dimensional beam, plane stress condition exists and also width in y-direction is stress-free. Hence we can set $\sigma_z = \sigma_y = \tau_{yz} = \tau_{xy} = \gamma_{yz} = \gamma_{xy} = 0$, while $\varepsilon_z \neq 0; \varepsilon_y \neq 0$. Also, for electric fields, we can assume $E_x = E_y = 0$. Only the coupling between longitudinal displacement and transverse electric filed is considered here. Using these conditions in constitutive equation (6), we get:

$$\begin{bmatrix} \sigma_x \\ \tau_{xz} \\ D_z \end{bmatrix} = \begin{bmatrix} \tilde{Q}_{11} & 0 & -\tilde{e}_{31} \\ 0 & \tilde{Q}_{55} & 0 \\ \tilde{e}_{31} & 0 & \tilde{\in}_3 \end{bmatrix} \begin{bmatrix} \varepsilon_x \\ \gamma_{xz} \\ E_z \end{bmatrix} \tag{7}$$

where $\tilde{Q}_{11} = Q_{11} - \left(Q_{12}^2 / Q_{22}\right)$, $\tilde{Q}_{55} = Q_{55}$ and $Q_{ij} = C_{ij} - \left(\frac{C_{i3} C_{j3}}{C_{33}}\right)$ $(i, j = 1,2,4,5,6)$;

$\tilde{e}_{31} = \bar{e}_{31} - \bar{e}_{32}\left(\frac{Q_{12}}{Q_{22}}\right)$ and $\bar{e}_{3i} = e_{3i} - e_{33}\left(C_{i3}/C_{33}\right)(i = 1,2)$;

$\tilde{\in}_3 = \bar{\in}_3 + \left(\bar{e}_{32}^2 / Q_{22}\right)$ and $\bar{\in}_3 = \in_3 + \left(e_{33}^2 / C_{33}\right)$.

4 DERIVATION OF ELECTRIC POTENTIAL CONSISTENT WITH FSDT

For the free volumic charge density assumption, the electrostatic equilibrium equation of i^{th} piezoelectric layer reduces to:

$$\frac{\partial D_z^i}{\partial z} = 0 \tag{8}$$

as $D_x = D_y = 0$ from equation (7).

Using equations (3), (5), (7) and (8), we get:

$$\frac{\partial^2 \varphi_i}{\partial z^2} = \frac{\tilde{e}_{31}^i}{\tilde{\in}_3^i} \theta' \tag{9}$$

On solving equation (9), we have:

$$\varphi_i(x,z) = \frac{\tilde{e}_{31}^i}{\tilde{\epsilon}_3^i}\frac{z^2}{2}\theta'(x) + C_1(x)z + C_2 \tag{10}$$

where C_1 and C_2 are the constants to be obtained from boundary conditions for $\varphi(x,z)$ in z-direction. For i^{th} piezolayer boundary conditions are $\varphi_{(z=z_{i+1})} = \phi_{i+1}$ and $\varphi_{(z=z_i)} = \phi_i$. After solving equation (10) and simplifying, we get:

$$\varphi_i(x,z) = \bar{\varphi}_i(x) + \left(\frac{z-\bar{z}_i}{h_i}\right)\tilde{\varphi}_i(x) - \frac{\tilde{e}_{31}^i}{\tilde{\epsilon}_3^i}\frac{h_i^2}{8}\left(1 - \frac{4(z-\bar{z}_i)^2}{h_i^2}\right)\theta'(x) \tag{11}$$

where $\bar{\varphi}_i = (\phi_{i+1} + \phi_i)/2$; $\tilde{\varphi}_i = (\phi_{i+1} - \phi_i)$; and $\bar{z}_i = (z_{i+1} + z_i)/2$.

Form equation (11), it is clear that, electric potential consistent with FSDT mechanical field is quadratic in transverse direction. The first two terms which describe the linear part i.e. $\bar{\varphi}_i$ and $\tilde{\varphi}_i$ are the average and difference of potential on top and bottom faces of i^{th} piezolayer, respectively. The third term which is coupled quadratic denotes the contribution of bending deformation to the potential. The quadratic term constitutes the 'induced potential'. This derived field is different from that given by Benjeddou et al. (1997), which is based on Euler-Bernoulli beam theory and hence not suitable for beams where the shear effect is dominant. The coefficient of the induced potential term depends on geometric and material properties of the piezoelectric layer. Smart beams with thick piezolayers show considerable shear contribution to the induced potential.

The transverse electric field can be derived from equation (11) as:

$$E_z^i = -\frac{\partial\varphi_i(x,z)}{\partial z} = -\frac{\tilde{\varphi}_i(x)}{h_i} - \frac{\tilde{e}_{31}^i}{\tilde{\epsilon}_3^i}(z-\bar{z}_i)\theta'(x) \tag{12}$$

5 VARIATIONAL FORMULATION

Hamilton's principle is used to formulate piezoelectric smart beam. It is expressed as (Chee et al., 1999):

$$\delta\int_{t_1}^{t_2}(K - H + W)\,dt = \int_{t_1}^{t_2}(\delta K - \delta H + \delta W)\,dt = 0 \tag{13}$$

where, K =kinetic energy, H =potential energy and W =external work.

5.1 Variation of potential energy

For the j^{th} conventional material layer the variation of mechanical strain energy is given as (Chee et al., 1999):

$$\delta H_j = \int_V (\sigma_x^j \delta\varepsilon_x^j + \tau_{xz}^j \delta\gamma_{xz}^j) dV \tag{14}$$

The electromechanical energy variation for the i^{th} piezoelectric layer is given as (Chee et al., 1999):

$$\delta H_i = \int_V (\sigma_x^i \delta\varepsilon_x^i + \tau_{xz}^i \delta\gamma_{xz}^i - D_z^i \delta E_z^i) dV \tag{15}$$

Substituting the values of axial strain (ε_x), shear strain (γ_{xz}), transverse electric field (E_z), from equations (3), (4), (12) and using them along with constitutive relations from equation (7) in equations (14) and (15), the total potential energy variation of the piezoelectric smart beam can be written as:

$$\int_{t_1}^{t_2} \delta H \, dt = \int_{t_1}^{t_2}\int_x \left\{ \begin{array}{l} \delta u_0' \left(\left(\tilde{Q}_{11}^k I_0^k\right) u_0' + \left[\tilde{Q}_{11}^k I_1^k + \frac{(\tilde{e}_{31}^i)^2}{\tilde{\in}_3^i}\left(I_1^i - I_0^i \bar{z}_i\right)\right]\theta' + \left(\frac{\tilde{e}_{31}^i I_0^i}{h_i}\right)\tilde{\varphi}_i \right) \\ +\delta\theta' \left(\begin{array}{l} \left[\tilde{Q}_{11}^k I_1^k + \frac{(\tilde{e}_{31}^i)^2}{\tilde{\in}_3^i}\left(I_1^i - I_0^i \bar{z}_i\right)\right] u_0' + \left[\tilde{Q}_{11}^k I_2^k + \frac{(\tilde{e}_{31}^i)^2}{\tilde{\in}_3^i}\left(I_2^i - I_0^i \bar{z}_i^2\right)\right]\theta' \\ + \left(\frac{\tilde{e}_{31}^i I_0^i \bar{z}_i}{h_i}\right)\tilde{\varphi}_i \end{array} \right) \\ +\delta\theta\left[\left(\tilde{Q}_{55}^k I_0^k\right)\left(\theta + w_0'\right)\right] + \delta w_0'\left[\left(\tilde{Q}_{55}^k I_0^k\right)\left(\theta + w_0'\right)\right] + \\ +\delta\tilde{\varphi}_i \left(\left(\frac{\tilde{e}_{31}^i I_0^i}{h_i}\right) u_0' + \left(\frac{\tilde{e}_{31}^i I_0^i \bar{z}_i}{h_i}\right)\theta' - \left(\frac{\tilde{\in}_3^i I_0^i}{h_i^2}\right)\tilde{\varphi}_i \right) \end{array} \right\} dx\, dt \tag{16}$$

where i =(1.....number of piezoelectric layers in beam) and k =(1.....number of total layers in beams) and $I_q^k = b\frac{z_{k+1}^{q+1} - z_k^{q+1}}{q+1}$.

From equation (16), it is clear that the induced potential changes the stiffness of the piezoelectric smart beam.

5.2 Variation of kinetic energy

Total kinetic energy of the beam is given as:

$$K = \frac{1}{2} b \int_x \int_{z_k}^{z_{k+1}} \rho_k \left(\dot{u}^2 + \dot{w}^2 \right) dz\, dx \tag{17}$$

where ρ_k =volumic mass density of k^{th} layer in kgm^{-3} and k =(1.....number of total layers in beams). Substituting values of u and w from equations (1) and (2) and applying variation, to derive at:

$$\int_{t_1}^{t_2} \delta K\, dt = -\rho_k \int_{t_1}^{t_2} \int_x \left\{ \delta u_0 \left(I_0^k \ddot{u}_0 + I_1^k \ddot{\theta} \right) + \delta\theta \left(I_1^k \ddot{u}_0 + I_2^k \ddot{\theta} \right) + \delta w_0 \left(I_0^k \ddot{w}_0 \right) \right\} dx\, dt \tag{18}$$

where $\dot{()}$ denotes $\partial/\partial t$.

5.3 Variation of work of external forces

Total virtual work of the structure can be defined as product of virtual displacements with forces for the mechanical work and the product of the virtual electric potential with the charges for the electrical work. The variation of total work done by external mechanical and electrical loading is given by (Chee et al., 1999):

$$\int_{t_1}^{t_2} \delta W\, dt = \int_{t_1}^{t_2} \left\{ \begin{array}{l} \int_V \left(\delta u f_u^V + \delta w f_w^V \right) dV + \int_S \left(\delta u f_u^S + \delta w f_w^S \right) dS + \\ \sum \left(\delta u f_u^C + \delta w f_w^C \right) - \int_{S_\varphi} \delta\varphi\, q_0\, dS_\varphi \end{array} \right\} dt \tag{19}$$

in which f^V, f^S, f^C are volume, surface and point forces, respectively. q_0 and S_φ are the charge density and area on which charge is applied.

6 FINITE ELEMENT FORMULATION

Using the variational formulation described above, the finite element description of the problem can be developed. The two-noded beam element considered here is based on ESL-FSDT with layerwise electric potential in transverse direction. For the finite element formulation degrees of freedom consist of three mechanical (u_0, θ, w_0) and layerwise electrical variables $\tilde{\varphi}_i$ where (i =1.....number of piezoelectric layers). From the variational formulation it is clear that all variables are C^0 continuous, hence are modeled with standard Lagrange shape functions:

$$\left.\begin{aligned} u_0 &= \sum_{j=1}^{2} N_j(\xi) u_0^j;\ \theta = \sum_{j=1}^{2} N_j(\xi)\theta_j; \\ w_0 &= \sum_{j=1}^{2} N_j(\xi) w_0^j;\ \tilde{\varphi}_i = \sum_{j=1}^{2} N_j(\xi)\tilde{\varphi}_i^j; \end{aligned}\right\} \tag{20}$$

where $N_1 = \dfrac{1-\xi}{2}$ and $N_2 = \dfrac{1+\xi}{2}$; ξ is generalized (local) coordinate while x is global coordinate along the length of beam. The transformation between ξ and x is given as $\xi = 2(x - x_1)/(x_2 - x_1) - 1$ and $(x_2 - x_1) = l$, length of beam element. So, each element will have three mechanical and i electrical degrees of freedom per node namely $\left\{u_0, \theta, w_0, \tilde{\varphi}_i\right\}$.

Now the variation on basic mechanical and electrical variables can be transferred to nodal degrees of freedom. Substituting equation (20) in equations (16), (18), (19) and using them in equation (13), the following discretized form of model can be obtained:

$$\begin{bmatrix} [M] & 0 \\ 0 & 0 \end{bmatrix} \begin{bmatrix} \{\ddot{U}\} \\ \{\ddot{\Phi}\} \end{bmatrix} + \begin{bmatrix} [K_{uu}] & [K_{u\varphi}] \\ [K_{\varphi u}] & [K_{\varphi\varphi}] \end{bmatrix} \begin{bmatrix} \{U\} \\ \{\Phi\} \end{bmatrix} = \begin{bmatrix} \{F\} \\ \{Q\} \end{bmatrix} \tag{21}$$

where M is mass matrix, $K_{u\varphi}, K_{u\varphi}, K_{\varphi u}, K_{\varphi\varphi}$ are global stiffness sub-matrices. U, Φ are the global mechanical displacement and electric potential degrees of freedom vector, respectively. F and Q are global mechanical and electrical force vectors, respectively. Now the general formulation has been converted to matrix equation which can be solved according to electrical conditions (open/closed circuit), configuration (actuator/sensor) and type of analysis (static/dynamic).

7 NUMERICAL EXAMPLES AND DISCUSSIONS

The developed formulation has been coded in MATLAB environment. The numerical experiments for validation are carried out for static (actuation/sensing) and modal analyses. The effect of induced potential on static and modal behaviour of smart structure is studied. The present formulation is validated by comparing the test results with those from conventional formulation and 2D ANSYS FE simulations. For ANSYS simulations, PLANE 223 elements are used for modeling piezoelectric layer and PLANE 183 elements for conventional material. The finite elements available in the literature which employ ESL- FSDT with layerwise linear electric potential (LP) distribution like Narayanan and Balamurugan, (2003) are designated here as FSDT-LP. For the purpose of comparing the accuracy of results, FSDT-LP results with no sublayers and with a sufficient number of sublayers per piezoelectric physical layer (four sublayers/piezolayer) are considered. The present formulation employing ESL-FSDT with layerwise consistent potential is designated as

FSDT-CP. The present HSDT-CP element models the piezoelectric physical layer as a single layer and does not employ sublayers.

An extension mode piezoelectric beam structure is studied for different proportions of piezoelectric material in the total thickness of the beam, to capture the effect of geometry on the induced potential. A smart beam with oppositely poled piezoelectric layers symmetrically bonded to the aluminum host layer as shown in Figure 2, is studied here. This three layered bender has been studied by numerous researchers using different material and geometric properties for sensor and actuator configurations.

The material properties of the beam are (Kapuria and Hagedorn, 2007):

Aluminum: $E = 70.3GPa; \nu = 0.345; \rho = 2710\ kgm^{-3}$

PZT 5H:

$C_{11} = C_{22} = 126GPa; C_{12} = 79.5GPa; C_{13} = C_{23} = 84.1GPa; C_{33} = 117GPa; C_{44} = C_{55} = 23GPa;$

$C_{66} = 23.25GPa; e_{31} = e_{32} = -6.5Cm^{-2}; e_{33} = 23.3Cm^{-2}; \in_3 = 1.3\times10^{-8}\ Fm^{-1}; \rho = 7500kgm^{-3}$

The length and total height of the beam are taken constant with values $L = 100mm$ and $h = 10mm$, respectively while the thickness of piezoelectric layer h_p and aluminum layer h_{al} are varied.

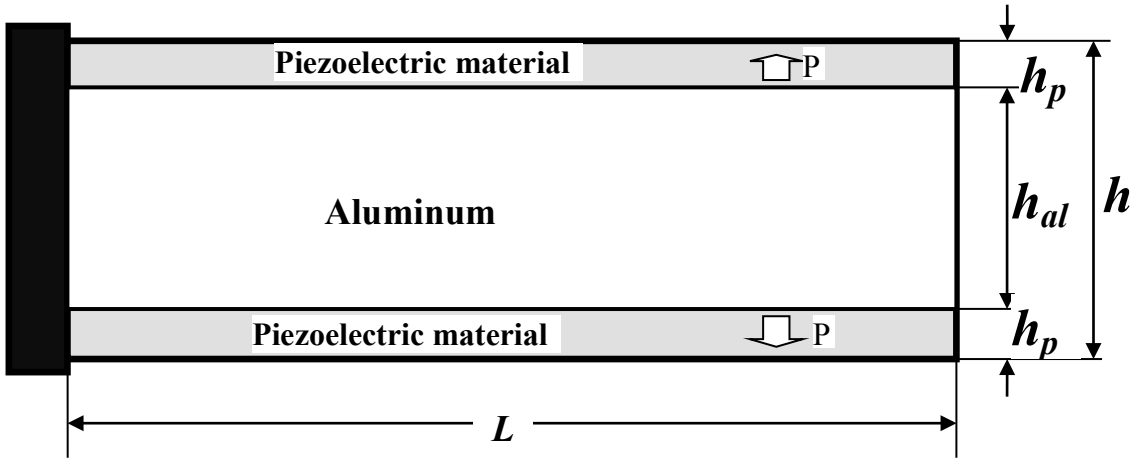

Figure 2 Three layered cantilever beam with symmetrically bonded piezoelectric layers in extension mode.

7.1 Static analysis: Actuator configuration:

In order to bend the beam, the voltages of $\pm10volts$ are applied to top and bottom faces of top and bottom surface piezoelectric layers, respectively while the interfaces with aluminum layer are grounded.

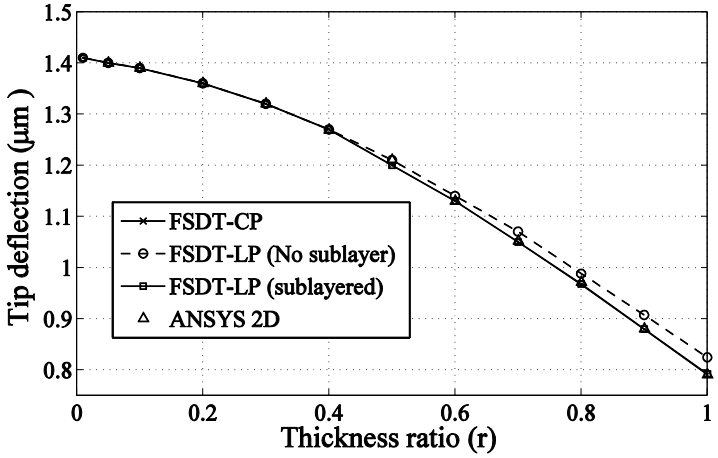

Figure 3 Actuator configuration: Variation of tip deflection of three layered cantilever with thickness ratio.

The results obtained by present FSDT-CP and FSDT-LP of (Narayanan and Balamurugan, 2003) are compared for various thickness ratios $\left(r = 2h_p/h\right)$. The results for tip deflection of the cantilever, plotted in Figure 3, show that FSDT-CP results closely match with ANSYS 2D simulation results for all regimes of thickness ratios. A refined mesh of 100x40 elements has been used for obtaining converged 2D analysis results. It is observed that FSDT-LP solutions deviate considerably from actual solutions when the piezoelectric material dominates the structure. It shows the inadequacy of FSDT-LP to take care of higher order through-thickness electric potential distribution. In order to yield accurate results FSDT- LP demands sublayers in modelling of each piezoelectric layer. This obsevation is in consistent with findings of Rachmadini et al. (2005) which emphasize on the dicretization of the piezoelectric layer in the transverse direction to get accurate results.

Also, the variation of error (%) in tip deflection with thickness ratio, due to use of FSDT-LP with single layer modeling of piezoelectric layer is plotted in Figure 4.

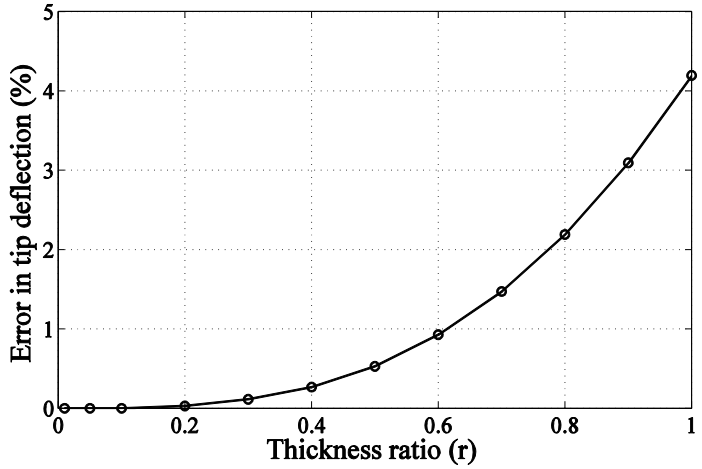

Figure 4 Actuator configuration: Variation of error (%) in tip deflection of three layered cantilever smart beam with thickness ratio due to use of FSDT-LP.

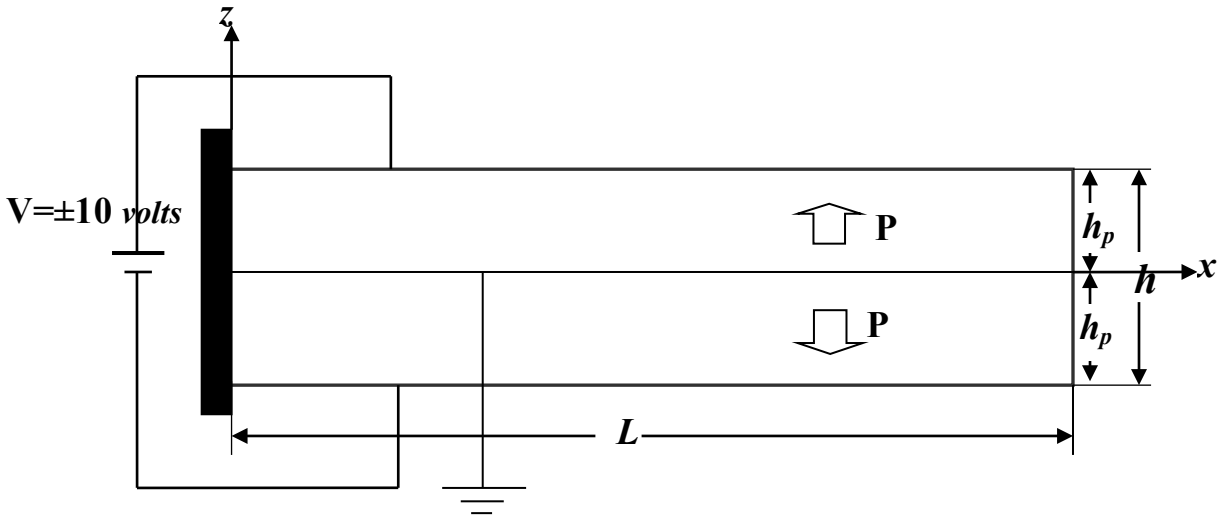

Figure 5 Bimorph cantilever in actuator configuration.

Figure 4 shows that as we move from a beam of purely core material to piezoelectric material, the error (%) increases significantly being highest for bimorph (r=1). Hence, the bimorph configuration shown in Figure 5 is chosen for further detailed investigation.

Table 1 shows the results for the tip deflection of the bimorph configuration for different numbers of sublayers in modeling with FSDT-LP. As seen from results, only sublayered model gives the accurate prediction of tip deflection as of FSDT-CP and ANSYS 2D results.

Table 1 Actuator configuration: Tip deflection of the bimorph cantilever ($h = 10\,mm;\ L = 100\,mm$)

Formulation	Tip deflection (μm)
ANSYS 2D	0.790
FSDT CP	0.790
FSDT LP	
No sublayers	0.824
2 sublayers/layer	0.798
4 sublayers/layer	0.792

Figure 6 shows the comparison of transverse deflection results obtained with FSDT-CP, FSDT-LP and ANSYS 2D simulation for the bimorph. For ANSYS 2D simulation a mesh size of 100x5 per layer is used to model the bimorph. FSDT CP results match closely with ANSYS 2D simulation while FSDT-LP results can only be improved by the addition of sublayers.

As shown in Figure 7, the through-thickness distribution of electric potential is nonlinear and present FSDT-CP captures the accurate behaviour without any sublayers unlike FSDT-LP.

The axial stress developed in the bimorph cantilever is plotted in Figure 8, which is discontinuous and maximum at the interface. It is seen that FSDT-LP under predicts the maximum value and requires sublayers to reach the actual value as predicted by FSDT-CP and ANSYS 2D simulation.

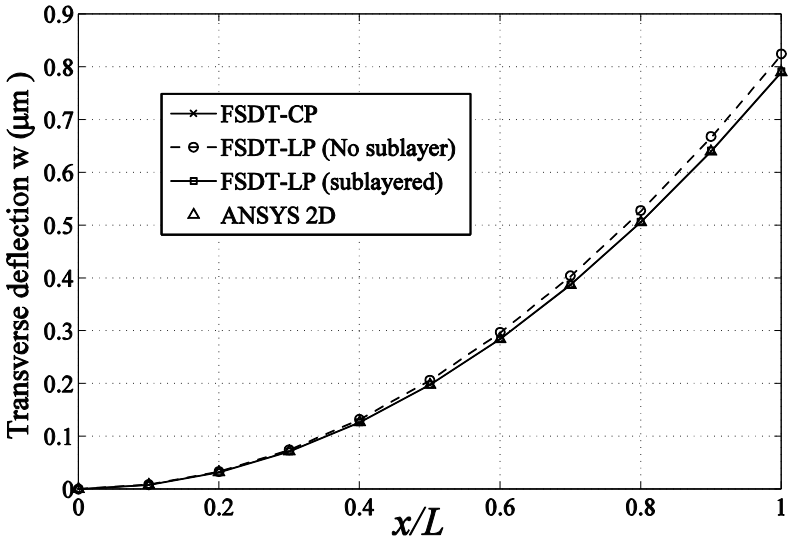

Figure 6 Actuator configuration: Transverse deflection of the bimorph cantilever along the length.

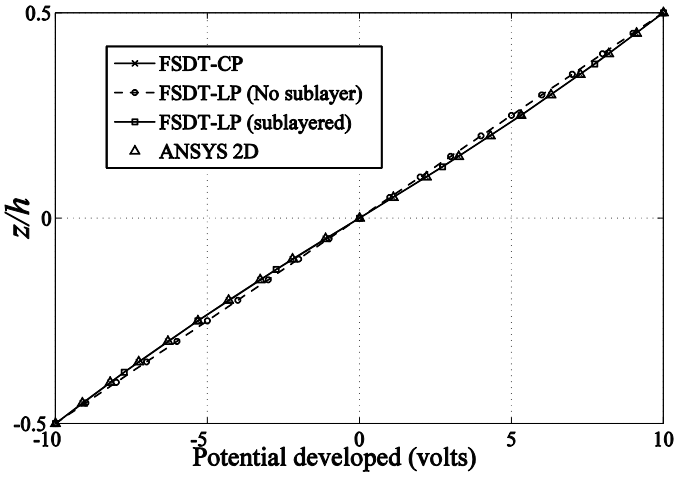

Figure 7 Actuator configuration: Through-thickness potential distribution of the bimorph cantilever.

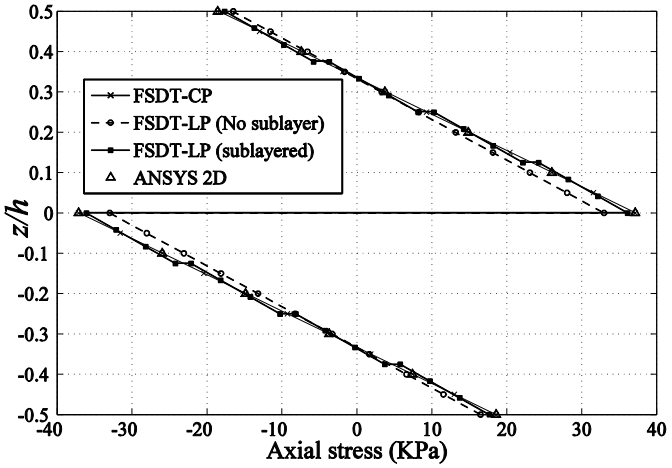

Figure 8 Actuator configuration: Through-thickness axial stress distribution in the bimorph cantilever.

7.2 Static analysis: Sensor configuration

The three layered cantilever beam shown in Figure 2 is subjected to a tip load of -1000 N, to validate the present formulation for sensor configuration. The results for tip deflection and potential developed at mid-span are plotted in Figures 9 and 10, for various thickness ratios of three layered cantilever smart beam.

From Figures 9 and 10, it is clear that FSDT-CP is able to yield accurate results as that of ANSYS 2D simulation and sublayered version of FSDT-LP. Also, the variation of error (%) in results for tip deflection and potential developed by FSDT-LP (no sublayers) with thickness ratio in the same case is plotted in Figure 11. It is found that for a given thickness ratio, the percentage error in tip deflection and the developed potential are same. The error (%) grows from zero for conventional material to maximum for purely piezoelectric material i.e. bimorph. Hence the bimorph shown in Figure 12 is studied in detail.

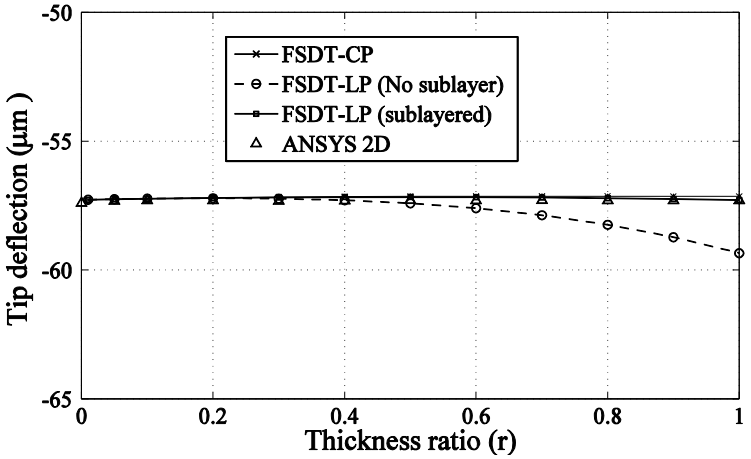

Figure 9 Sensor configuration: Variation of tip deflection of three layered cantilever with thickness ratio.

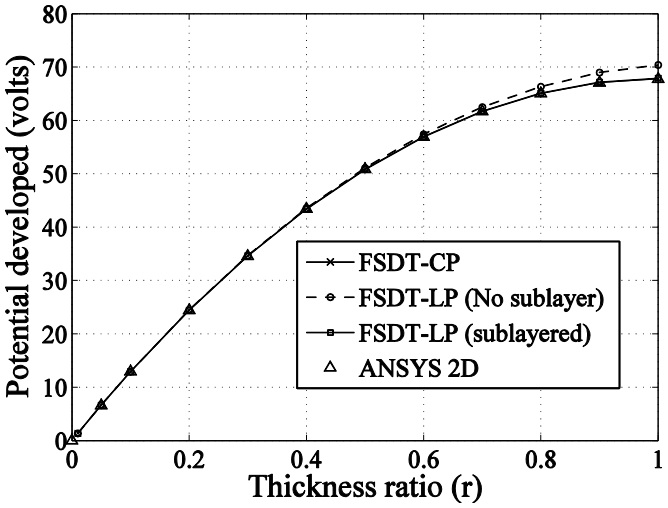

Figure 10 Sensor configuration: Variation of potential developed in each piezoelectric layer at mid-span of three layered cantilever with thickness ratio.

Table 2 shows the results for tip deflection and potential developed across each piezoelectric layer at mid-span of the bimorph for various sublayers in modeling of FSDT-LP. From the tabulated results it can be seen that, with the addition of sublayers in modeling of FSDT-LP the error in predicting accurate value decreases.

The results obtained by FSDT-CP, FSDT-LP with and without sublayers and ANSYS 2D simulation, for transverse deflection and potential developed across each layer along the length of the bimorph are plotted in Figures 13 and 14, respectively. For ANSYS 2D simulation, a refined mesh of 100x5 per layer is used.

The through-thickness potential distribution at mid-span is plotted in Figure 15 for the bimorph cantilever. FSDT-LP without sublayers shows linear distribution and with the addition of sublayers in model, reaches the actual distribution as predicted by the ANSYS 2D simulation and FSDT-CP. This proves ability of FSDT-CP to capture accurate through-thickness distribution of electric potential without using sublayers.

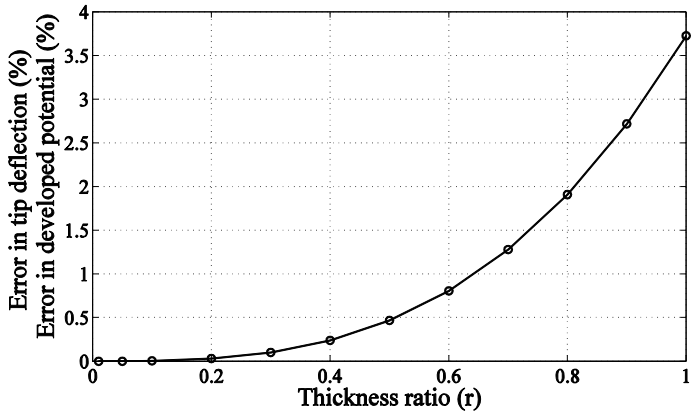

Figure 11 Sensor configuration: Variation of error (%) in tip deflection and developed potential of three layered cantilever smart beam with thickness ratio due to use of FSDT-LP.

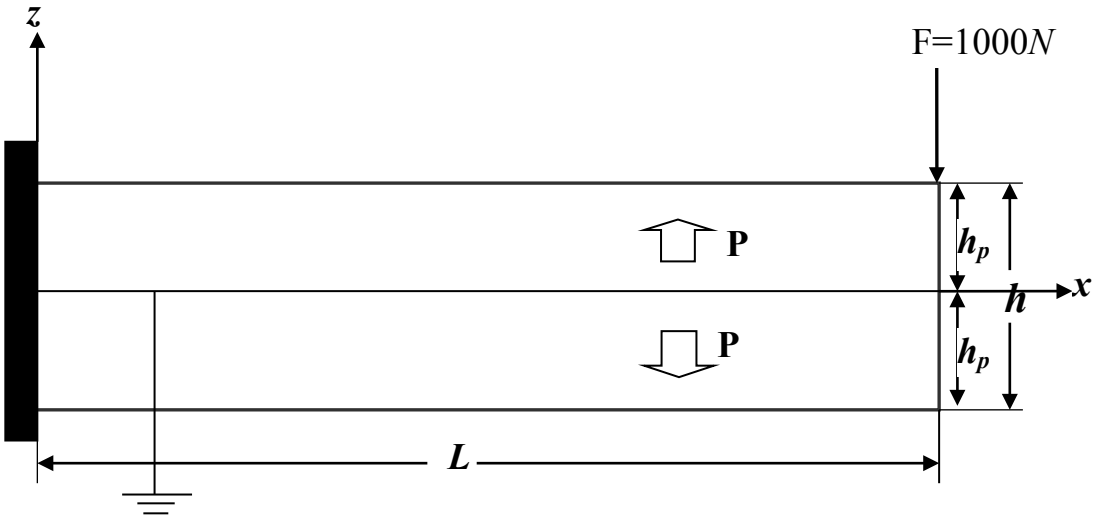

Figure 12 Bimorph cantilever in sensor configuration.

Table 2 Sensor configuration: Tip deflection and potential developed at mid-span of the bimorph cantilever ($h = 10\,mm;\ L = 100\,mm$)

Formulation	Tip deflection (μm)	Developed potential
ANSYS 2D	-57.2	67.76
FSDT CP	-57.2	67.76
FSDT LP		
No sublayers	-59.3	70.38
2 sublayers/layer	-57.7	68.40
4 sublayers/layer	-57.3	67.91

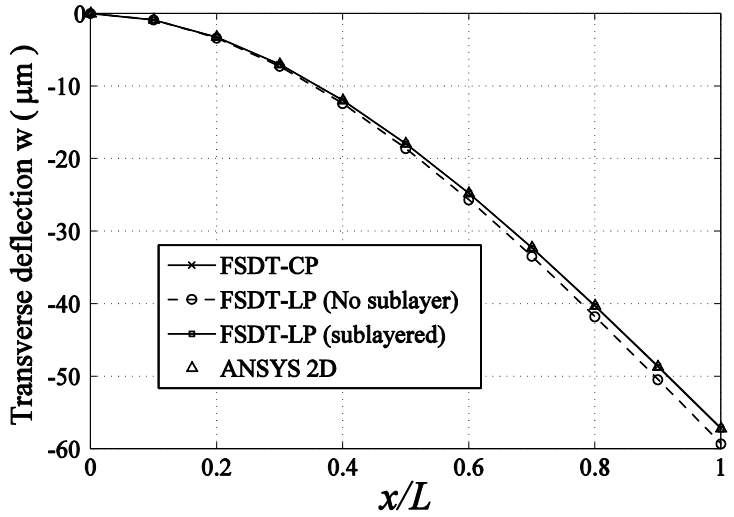

Figure 13 Sensor configuration: Transverse deflection of the bimorph cantilever along the length.

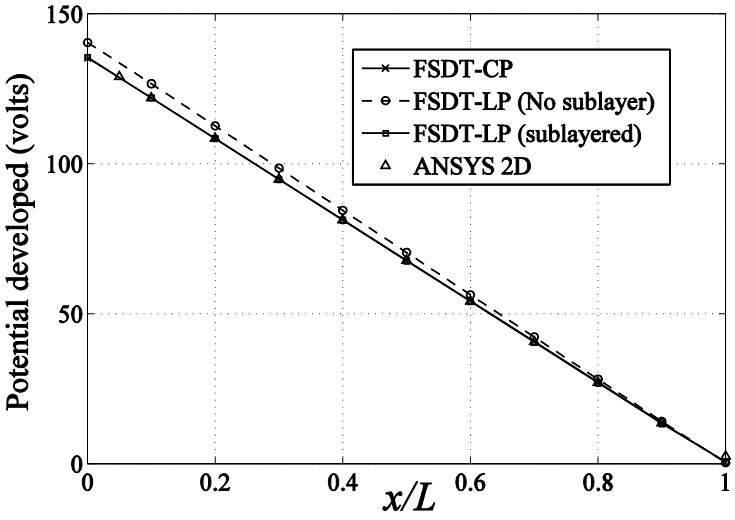

Figure 14 Sensor configuration: Developed potential across each piezoelectric layer of the bimorph cantilever along the length.

The through-thickness axial stress distribution at the root of the bimorph has been plotted in Figure 16. As seen from the plot, FSDT-LP under predicts the maximum value developed at the top and bottom surfaces and shows discontinuity of the stress profile at the interface. These deficiencies are removed by sublayered model which approaches the actual distribution as predicted by FSDT-CP and ANSYS 2D simulation.

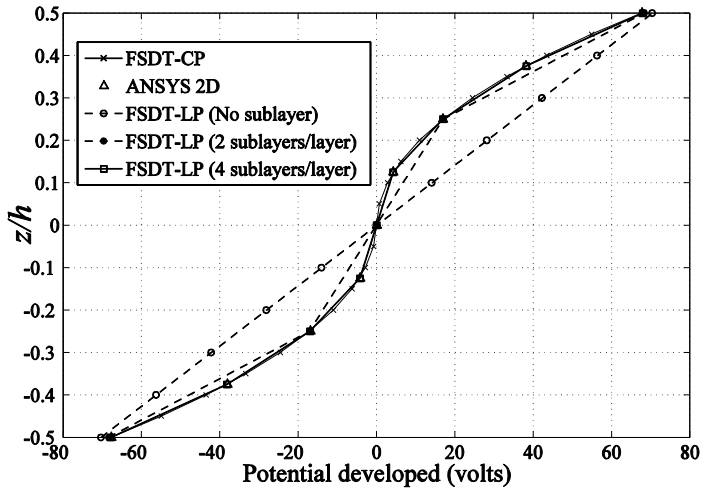

Figure 15 Sensor configuration: Through-thickness potential distribution at mid-span of the bimorph cantilever.

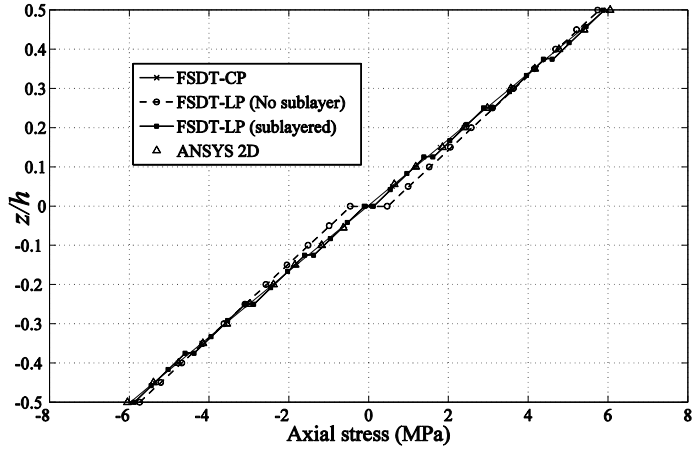

Figure 16 Sensor configuration: Through-thickness axial stress distribution at the root of the bimorph cantilever.

7.3 Modal analysis

The FSDT-CP is validated here for its accuracy to predict the natural frequencies of piezoelectric extension mode smart beams. The numerical experiments are carried out for open and closed circuit electrical boundary conditions. The three layered cantilever beam shown in Figure 2 is evaluated here. For closed boundary condition, both top and bottom faces of each piezoelectric layer are grounded while for open circuit condition only interfaces with aluminum layer are grounded and the other faces are left free.

The variation of first natural frequencies with thickness ratio for the three layered cantilever beam in open and closed circuit electrical conditions are plotted in Figures 17 and 18, respectively. Present FSDT-CP gives accurate predictions of natural frequencies. The deterioration of accuracy of FSDT-LP (without sublayers) results with thickness ratio is evident from Figure 19.

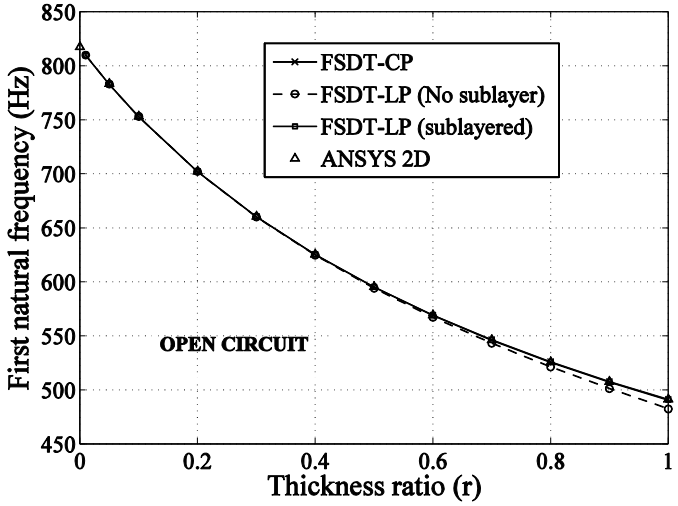

Figure 17 Variation of first natural frequency of three layered cantilevered smart beam with thickness ratio in open circuit electrical boundary condition.

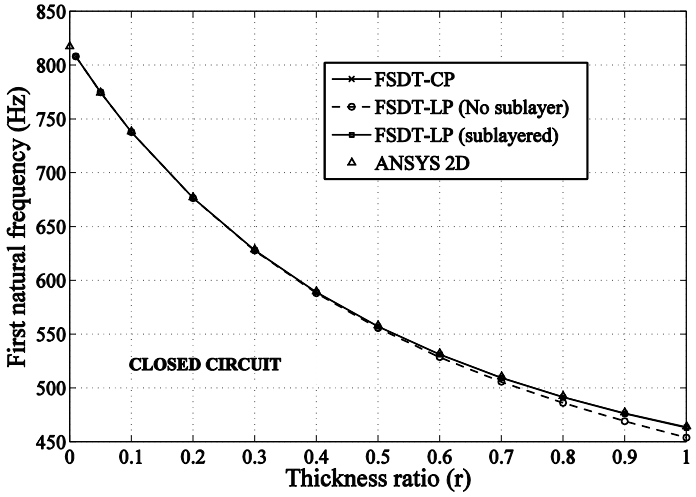

Figure 18 Variation of first natural frequency of three layered cantilevered smart beam with thickness ratio in closed circuit electrical boundary condition.

As seen from Figure 19, the maximum error occurs when the beam is made up of purely piezoelectric material i.e. bimorph. The first three natural frequencies for the bimorph cantilever in both electrical boundary conditions obtained by FSDT-CP, FSDT-LP with and without sublayers and ANSYS 2D simulation are tabulated in Table 3. As seen from the results, the FSDT-CP yields accurate natural frequencies without sublayers, unlike FSDT-LP. The first three natural bending modes for the bimorph are plotted in Figure 20.

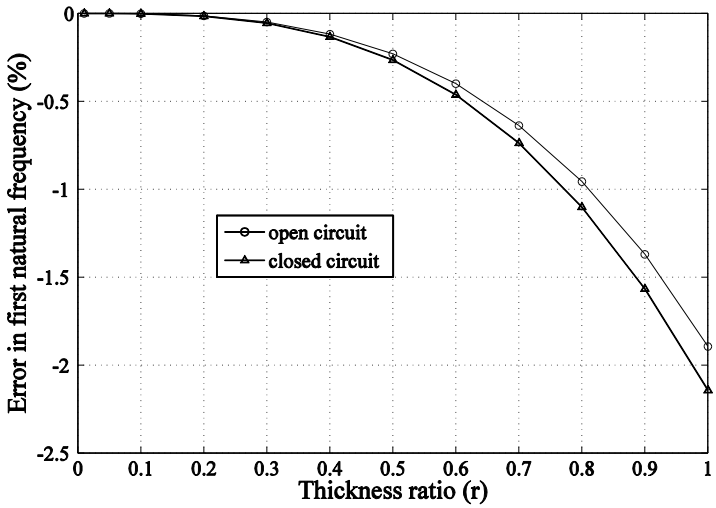

Figure 19 Variation of error (%) in first natural frequency of three layered cantilever smart beam with thickness ratio due to use of FSDT LP.

Table 3 Natural frequencies of the bimorph cantilever ($h = 10\,mm;\ L = 100\,mm$)

Formulation	Natural frequencies (Hz)					
	Open Circuit			Closed Circuit		
	1st	2nd	3rd	1st	2nd	3rd
FSDT CP	491.5	2949	7666	463.5	2792	7072
ANSYS	491.3	2929	7658	464.3	2783	7093
FSDT LP (no sublayer)	482.4	2898	7650	453.8	2736	7072
FSDT LP (sublayered)	491.0	2944	7666	462.9	2788	7072

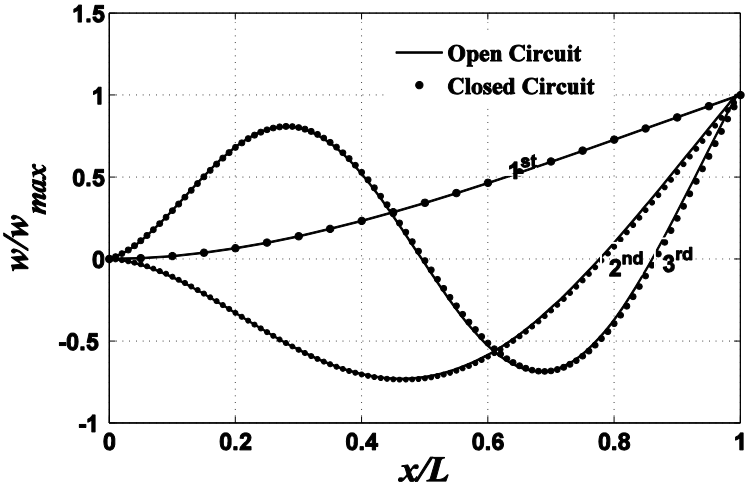

Figure 20 Natural bending modes of the bimorph cantilever.

8 CONCLUSION

In the present work, FSDT based variational formulation for piezoelectric beam in extension mode and its finite element implementation has been explained. A consistent quadratic through-thickness distribution of electric potential in a physical piezoelectric layer has been derived using an electrostatic equilibrium equation. This derived potential contains an addition to the conventional linear part, a higher order coupled term. The coefficient of the coupled term depends on geometric and material properties of the piezoelectric layer. This coupled term takes care of the induced potential effect and the associated change in stiffness. The formulation has been validated for static and modal analyses. Through numerical test problems, the accuracy and efficiency of the present formulation have been proved. The parametric study carried out in this work reveals the importance of considering the nonlinear nature of through-thickness electric potential distribution. Numerical errors due to the inadequate modeling of electric potential are very significant when the piezoelectric material dominates the structure. In conventional formulations, these errors can be minimized by adding sublayers in the modeling of piezoelectric layer and/or higher order representation of electric potential along thickness. But these remedies will add extra electrical degrees of freedom in finite element formulation, hence increasing computational efforts. Present formulation achieves the accu-

racy of a 2D finite element without bringing in any additional degrees of freedom with the help of coupled field representation of electric potential. This novel work provides an efficient way to reduce the 2D piezoelectric finite element to a truly 1D beam element, without sacrificing accuracy.

References

Abramovich, H., Pletner, B. (1997). Actuation and sensing of piezolaminated sandwich type structures, Composite Structures 38: 17-27.

Abramovich, H. (1998). Deflection control of laminated composite beams with piezoceramic layers - closed form solutions, Composite Structures 43: 217-231.

Aldraihem, O.J., Khdeir, A.A. (2000). Smart beams with extension and thickness-shear piezoelectric actuators, Smart Materials and Structures 9: 1-9.

Bendary, I.M., Elshafei M.A., Riad, A.M. (2010) Finite Element Model of Smart Beams with Distributed Piezoelectric Actuators, J. Intelligent Material Systems and Structures 21:747-758.

Benjeddou, A., Trindade, M.A., Ohayon, R. (1997). A unified beam finite element model for extension and shear piezoelectric actuation mechanisms, J. Intelligent Material Systems and Structures 8: 1012-1025.

Benjeddou, A., Trindade, M.A., Ohayon, R. (2000). Piezoelectric actuation mechanisms for intelligent sandwich structures, Smart Materials and Structures 9: 328-335.

Chee, C.Y.K., Tong, L., Steven, G.P. (1999). A mixed model for composite beams with piezoelectric actuators and sensors, Smart Materials and Structures 8: 417-432.

Crawley, E.F., de Luis, J. (1987). Use of piezoelectric actuators as elements of intelligent structures, AIAA J. 25: 1373-1385.

Donthireddy, P., Chandrashekhara, K. (1996). Modeling and shape control of composite beams with embedded piezoelectric actuators, Composite Structures 35: 237-244.

Elshafei, M.A., Alraiess, F. (2013). Modeling and analysis of smart piezoelectric beams using simple higher order shear deformation theory, Smart Materials and Structures 22: 35006-35019.

Hwang, W.S., Park, H.C. (1993). Finite element modeling of piezoelectric sensors and actuators, AIAA J. 31: 930-937.

Kapuria, S., Hagedorn, P. (2007). Unified efficient layerwise theory for smart beams with segmented extension/shear mode, piezoelectric actuators and sensors, J. Mechanics of Materials and Structures 2: 1267-1298.

Khdeir, A.A., Aldraihem, O.J. (2001). Deflection analysis of beams with extension and shear piezoelectric patches using discontinuity functions, Smart Materials and Structures 10: 212-220.

Narayanan, S., Balamurugan, V. (2003). Finite element modelling of piezolaminated smart structures for active vibration control with distributed sensors and actuators, J. Sound and Vibration 262: 529–562.

Neto, M.A., Yu, W., Roy, S. (2009). Two finite elements for general composite beams with piezoelectric actuators and sensors, Finite Elements in Analysis and Design 45: 295-304.

Peng, X.Q., Lam, K.Y., Liu G.R. (1998). Active vibration control of composite beams with piezoelectrics: A finite element model with third order theory, J. Sound and Vibration 209: 635-650.

Plagianakos, T.S., Saravanos, D.A. (2005). Coupled high-order shear layerwise analysis of adaptive sandwich piezoelectric composite beams, AIAA J. 43: 885-894.

Rachmadini, Y., Lee, S., Park H.C., Yoon, K.J., Goo, N.S. (2005). The effect of electro-mechanical coupling stiffness on the through-the-thickness electric potential distribution of piezoelectric actuators, Smart Materials and Structures 14: 754-758.

Raja, S., Pratap, G., Sinha, P.K. (2002). Active vibration control of composite sandwich beams with piezoelectric extension-bending and shear actuators, Smart Materials and Structures 11: 63-71.

Robbins, D.H., Reddy, J.N. (1991). Analysis of piezoelectrically actuated beams using a layer-wise displacement theory, Computers and Structures 41: 265–279.

Rathi, V., Khan, A.H., (2012). Vibration attenuation and shape control of surface mounted, embedded smart beam, Latin American Journal of Solids and Structures 9: 401-424.

Saravanos, D.A., Heyliger, P.R. (1995). Coupled layerwise analysis of composite beams with embedded piezoelectric sensors and actuators, J. Intelligent Material Systems and Structures 6: 350-363.

Shen, M.H.H. (1995). A new modeling technique for piezoelectrically actuated beams, Computers and Structures 57: 361-366.

Sun, B., Huang, D. (2000). Analytical vibration suppression analysis of composite beams with piezoelectric laminae, Smart Materials and Structures 9: 751-760.

Tzou, H.S., Tseng, C.I. (1988). Active vibration control of distributed parameter systems by finite element method, Computers in Engineering 3: 599-604.

Tzou, H.S., Tseng, C.I. (1991). Distributed vibration control and identification of coupled elastic/piezoelectric systems: finite element formulations and applications, Mechanical Systems and Signal Processing 5: 215-231.

Tzou, H.S., Ye, R. (1996). Analysis of piezoelastic structures with laminated piezoelectric triangle shell elements, AIAA J. 34: 110-115.

Zhang, X.D., Sun, C.T. (1996). Formulation of an adaptive sandwich beam, Smart Materials and Structures 5: 814-823.